Focusing Through Walls: An E-shaped Patch Antenna Improves Whole-Home Radio Tomography

Peter Hillyard*, Cheng Qi†, Amal Al-Husseiny*, Gregory D. Durgin† and Neal Patwari*‡
*University of Utah, {peter.hillyard,amal.yousseef}@utah.edu, npatwari@ece.utah.edu
†Georgia Institute of Technology, {chengqi,durgin}@gatech.edu
‡Xandem Technology

***Abstract*—Tagless identification and tracking with through-wall received signal strength-based radio tomographic imaging (RTI) allows emergency responders to learn where people are inside of a building before entering the building. Use of directional antennas in RTI nodes focuses RF power along the link line, improving system performance. However, antennas placed on a building's exterior wall can be detuned by their close proximity to the dielectric, thus sending power across wider angles and resulting in less accurate imaging. In this paper, we improve through-wall RTI by using an E-shaped patch antenna we design to be mounted to an exterior wall. Along with its directionality, the E-shaped patch antenna is designed to avoid impedance mismatches when brought into close proximity of a dielectric material, thus increasing radiation through the exterior wall and along the link line. From our experiments, we demonstrate that the E-shaped patch antenna can reduce the median root mean square localization error by up to 43% when compared to microstrip patch and omnidirectional antennas. For equal error performance, the E-shaped patch antenna allows an RTI system to reduce power and bandwidth usage by using fewer nodes and measuring on fewer channels.**

I. Introduction

First responders, security personnel, and tactical forces can operate with increased safety when they know where people are located in a building prior to entering the building. RF sensing has been a popular choice for localizing people through walls because of its ability to sense moving people through non-metallic obstructions, through smoke, in any lighting condition, and *without tags* [1]–[4]. Prior research has shown how radio tomographic imaging (RTI) provides a low power and low cost-per-unit solution for imaging motion through walls and buildings and thus locate people inside [1], [5], [6]. To use RTI in security scenarios, first responders deploy nodes around the perimeter of the building. Facilitating rapid (and thus safer) deployment of the nodes is of great importance. For example, a requirement for SWAT use of an RTI system is that the system is easily deployable to keep first responders safe [7]. We propose attaching nodes to the exterior wall as a means of making the system easily deployable. We envision first responders launching or opportunistically placing nodes directly on the exterior walls of a building. After the nodes are attached to the walls, the nodes record pairwise received signal strength (RSS) measurements, and an image map is estimated of the motion inside of the building.

There are particular challenges with RTI for through-wall imaging in these tactical scenarios. First, multipath fading does not always match the assumed spatial model. RTI is based on the assumption that changes in RSS on a link are due to the presence of a person on the *link line*, the imaginary line segment that connects the two nodes. If most of the power does not travel along the link line, then the person's presence on the link line does not have a strong impact on the RSS, thus degrading the accuracy of RTI. A second challenge is that, with nodes attached to a wall and their antenna main lobe directed through the wall, the antenna impedance can be detuned. The antenna's center frequency can shift and its radiation pattern can be altered. A detuned antenna results in high attenuation of the multipath components which travel along the link line. RTI's localization performance, in turn, is negatively affected by the model mismatch.

In this paper, we propose addressing these two challenges and improving localization performance of RTI by equipping nodes with an E-shaped patch antenna we specifically develop to be attached to an exterior building wall [8]. Our E-shaped patch antenna is a directional antenna that focuses most of its power through the wall to which it is attached and thereby amplifies multipath on or near the link line and attenuates those far from the link line.

Prior research has addressed the use of directional antennas for RTI [5], [6]. In particular, [5] used directional antennas for through-wall RTI, but localization accuracy results, in comparison to omnidirectional antennas, were mixed. We address this counter-intuitive result by showing that the classical microstrip patch antenna used in [5] is detuned when placed against common building materials. Our E-shaped patch antenna naturally has a wider operating bandwidth such that it is not strongly negatively affected when it is brought into close proximity to a dielectric material [9].

In experiments we perform, we compare the performance of our E-shaped patch antenna against both omnidirectional antennas and microstrip patch antennas at two different houses, one made of brick and the other of fiber cement siding. Both materials are known to have high RF losses, and thus through-wall localization should be particularly challenging. Using moving average-based and variance-based RTI [1], we show that the E-shaped patch antennas reduce the median root mean squared error (RMSE) by up to 43% compared to the omnidirectional and microstrip patch antennas. Alternatively, we demonstrate that we can deploy fewer nodes and measure fewer channels, and thus use less power and bandwidth, with

978-1-4799-1441-8/13/$31.00 © 2017 IEEE

the E-shaped patch antenna and achieve the same or lower median RMSE compared to the omnidirectional and microstrip patch antennas.

The remainder of this paper is organized as follows. In Section III, we describe the design and characteristics of the E-shaped patch antenna. We then describe in Section IV the two variations of RTI we use to test the influence of antenna type on localization performance. In Section V, we describe the two test locations and the experiments performed at those locations. We finish this paper by showing and evaluating the results of those experiments in Section VI.

II. Related Work

Being able to localize a person has opened many new technological advances. With RF tag-based localization, for example, a person wears or carries an RF tag or radio which can be localized with time of flight or signal strength measurements [10]. However, there are cases where localization is needed but a person or object may not have an RF tag. Device-free localization (DFL) [11], passive localization [12], or sensorless sensing [13] all describe the method of using wireless sensor networks to localize people without RF tags. Our work fits into this method type.

DFL is well-suited for security and first-response scenarios where entering a building can be life-threatening. Wireless RF devices are placed around the exterior of a building to "see" people inside. Ultra-wideband radars, for example, have been used to image the reflections a person creates from high-frequency pulses [2]–[4]. DFL is complementary to radar in that we image the location of a person, however, we form the image based on loss in received power (RSS) measured between many pairwise RF nodes which are deployed around the exterior of the building. One advantage of devices used for DFL is that the sensor signal power decays with distance d as $1/d^2$ as opposed to $1/d^4$ for radar. This means that to increase the sensing range for radars, the transmit power for radar must be increased dramatically more than devices used for DFL. This is a important design criteria for larger buildings with potentially many obstructions inside.

Many types of DFL have been proposed to perform through-wall localization including fingerprint-based methods [14], [15], particle filters [16], [17], and radio tomographic imaging (RTI) [18], [19]. Of these methods, RTI requires the least calibration and is computationally efficient. In our work, we explore the idea of using specially-made antennas that are attached to a wall to improve the localization accuracy of RTI. Prior research has addressed the use of directional antennas for RTI [5], [6]. In particular, [5] used directional antennas for through-wall RTI, but localization accuracy results, in comparison to omnidirectional antennas, were mixed. Our work expands upon these prior works by creating an antenna that does not become detuned when placed against an exterior wall. We show how our antenna improves the localization performance of RTI-based methods.

III. Antenna Comparison

When placed in close proximity with a dielectric material, an antenna with narrow bandwidth will have an impedance mismatch because of impedance detuning. This detuning results in a shift in the center frequency and losses in efficiency at the desired frequency. In contrast, the E-shaped patch antenna, as presented in [9], has several properties that make it an excellent fit for applications where the antenna is attached to the surface of an exterior wall. It is designed to maintain a wide bandwidth and reduce impedance mismatches. The E-shaped patch antenna is also designed to have a $75°$ horizontal half-power beamwidth and $80°$ vertical half-power beamwidth. This size of beam, when placed against an exterior wall, will direct most of the RF power into the building.

The E-shaped patch antenna is derived from a microstrip patch antenna which behaves like a cavity resonator, or equivalently, an LC resonant circuit. The outline of the E-shaped patch antenna is $L1$ by $W1$, with a feed point at $(W1/2, Lp)$, as shown in Fig. 1(a). The primary design feature of the E-shaped patch antenna is to introduce a secondary resonance by placing two identical slots with a length Ls and a width Ws into the microstrip patch antenna [8]. The slots are symmetrical on the feed point with distance Ds. We simulate and optimize the E-shaped patch antenna on an FR-4 dielectric with a relative permittivity of 3.66, a loss tangent of 0.0127 at 2.4 GHz, and thickness of 3.2mm (two layers of a 1.6mm thick substrates), using ANSYS HFSS software. The antenna is targeted to be 50 Ohm. Fig. 1(b) shows the E-shaped patch antenna fabricated on the same substrate with that in the simulation.

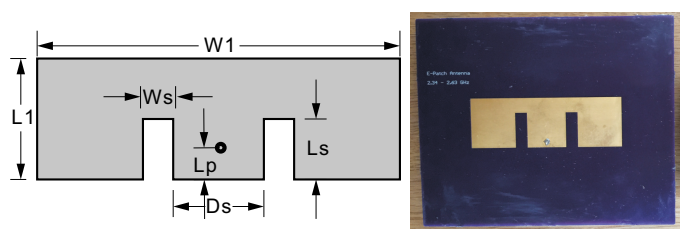

(a) Antenna Geometry (b) Antenna Photo

Fig. 1. (a) Geometry of a wide-band E-shaped patch antenna at $(W1/2, Lp)$ (b) Picture of fabricated E-shaped patch antenna targeted to be 50 Ohm

In this paper, we compare our E-shaped patch antenna to a commercially-available circular polarized microstrip patch antenna [20] and monopole antenna both of which are tuned to 2.4 GHz. These antennas are shown in Fig. 2. We present experimental values for the reflection coefficient of the E-shaped patch antenna, microstrip patch antenna, and omnidirectional antenna when in free space and when placed against a brick and cement board. The dielectric constant of the brick approximates to 3.58, and cement has a dielectric constant around 4.5. We show an example of our setup in Fig. 2. The reflection coefficient of the E-shaped patch antenna at 2.4 GHz, shown in Fig. 3, remains less than -10 dB for all materials, while that of the microstrip patch antenna, shown in

Fig. 2. A commercially-available monopole antenna (left) and a microstrip patch antenna (middle) are used to compare against our E-shaped patch antenna in RTI experiments. An example test setup (right) to collect reflection coefficient and radiation pattern data.

Fig. 3, exceeds -10 dB after detuning caused by the brick and cement board. Hence, the wideband E-shaped patch antenna is more robust in terms of reflection coefficient when placed upon various materials than the microstrip patch antenna. Fig. 3 also shows that the reflection coefficient of omnidirectional antenna remains less than -10 dB when attached to the brick but exceeds -10 dB after being detuned by the cement board.

We make some additional observations from Fig. 3. We first note that the microstrip patch antenna appears to have been tuned for 2.3 instead of 2.4 GHz. Since these are commercially available antennas, we had little control over their tuning. However, we note that all antennas have a return loss of -10 dB or lower at 2.4 GHz in freespace, meaning they are all at least 90% efficient in the operating frequency. In context of this paper, one of the most important observations is the detuning that occurs when the antenna is placed against the material. The omnidirectional and microstrip patch antenna are most negatively effected, whereas the E-shaped patch antenna improves. These improvements, though small in terms of efficiency, add up in big ways when evaluating antenna gains.

Fig. 4 presents the measured H-plane dB radiation patterns of the E-shaped patch, microstrip patch, and omnidirectional antenna in free space and attached to brick and cement board. Measurements were made with an open-air rooftop range using a network analyzer and a reference E-shape patch antenna. The E-shaped patch antenna has higher gain in free space than the ordinary microstrip patch antenna and omnidirectional antenna at 2.4 GHz. When attached to either the brick or cement board, the E-shaped patch antenna achieves higher directivity than the microstrip patch antenna and omnidirectional antenna. When attached to brick, the radiation pattern of the microstrip patch antenna degrades severely, while the E-shaped patch antenna maintains a similar radiation pattern as measured in free space. Furthermore, because free space has a higher impedance than that of brick and cement board, the omnidirectional antenna radiates more power into the materials than it does into free space. Therefore, omnidirectional antenna has higher gain than the microstrip patch antenna when attached to the materials.

IV. Radio Tomographic Imaging

In this section, we describe two algorithms for RTI that we use to compare localization performance when using different antennas.

The purpose of RTI is to create an image of an area of interest in order to locate an object or person inside. To that end, we deploy N nodes around the exterior periphery of a building. The nodes take turns transmitting a packet in a TDMA fashion. After all nodes have transmitted, each node has measured the RSS from all other nodes. We denote the RSS measured on link $l = (i, j, c)$ formed by transmitting node i and receiving node j on channel c as r_l. As a person moves inside the area of interest, new multipath are created while others are changed in phase and magnitude, which cause changes in r_l. We use a history of r_l to compute a link statistic y_l which quantifies the RSS change on link l. The link statistic from each link is sent to RTI to estimate an discretized image of where motion is observed. We describe two ways of computing link statistics in Section IV-A. First, we describe how the image is estimated.

In RTI, we want to estimate an $M \times 1$ image $\mathbf{x}$ from the link statistics stored in the $L \times 1$ vector $\mathbf{y} = [y_1, y_2, \ldots, y_L]^T$, where L is the number of links. The relationship between $\mathbf{y}$ and $\mathbf{x}$ has historically been modeled as the linear relationship

$$\mathbf{y} = \mathbf{A}\mathbf{x} + \mathbf{n} \tag{1}$$

where $\mathbf{A}$ is $L \times M$ and $\mathbf{n}$ is a $L \times 1$ noise vector. The (l, k) element of $\mathbf{A}$, $A_{l,k}$, quantifies the influence of pixel k on the link statistic for link l. We set $A_{l,k} = 1/p_l$ if $d^i_{l,k} + d^j_{l,k} < d_l + \lambda$ and zero otherwise, where $d^n_{l,k}$ is the distance from node n of link l to pixel k, d_l is the distance between the transmitting and receiving node of link l, λ is the ellipse width, and p_l is the number of pixels inside the link l ellipse.

Estimating the image $\mathbf{x}$ is an ill-posed problem. To address this issue, we use the regularized least-squares solution, which constrains the estimated image to be smooth [21]. The result of RTI is an image $\hat{\mathbf{x}}$. We choose the center coordinate of the pixel with the greatest value in $\hat{\mathbf{x}}$ to be the estimated location of the person. We show an image generated by RTI during one of the experiments in Fig. 5.

A. Link Statistics

An essential part of RTI is the computation of the link statistics vector $\mathbf{y}$. The elements of the vector represent that amount of change that has occurred in the RSS for each link. Some research has used the difference between the current RSS and the average RSS during an empty-room calibration period to compute the link statistics [18]. However, in emergency applications, it is unlikely we will have the opportunity to measure an empty-room average RSS. We alternatively describe two methods to compute link statistics by using a history of RSS measurements to quantify which links' RSS have recently changed. Although we avoid requiring an empty-room calibration, we note that these two methods cannot image people who are completely stationary.

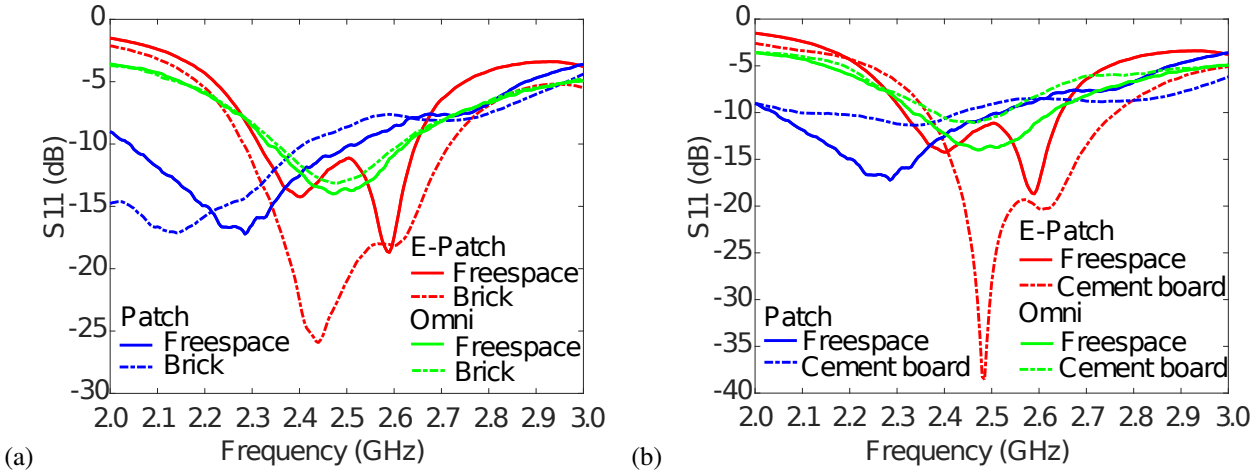

Fig. 3. Measured reflection coefficients (S11) for the E-shaped patch, the microstrip patch antenna, and the omnidirectional antenna in free space and attached to (a) brick and (b) cement board.

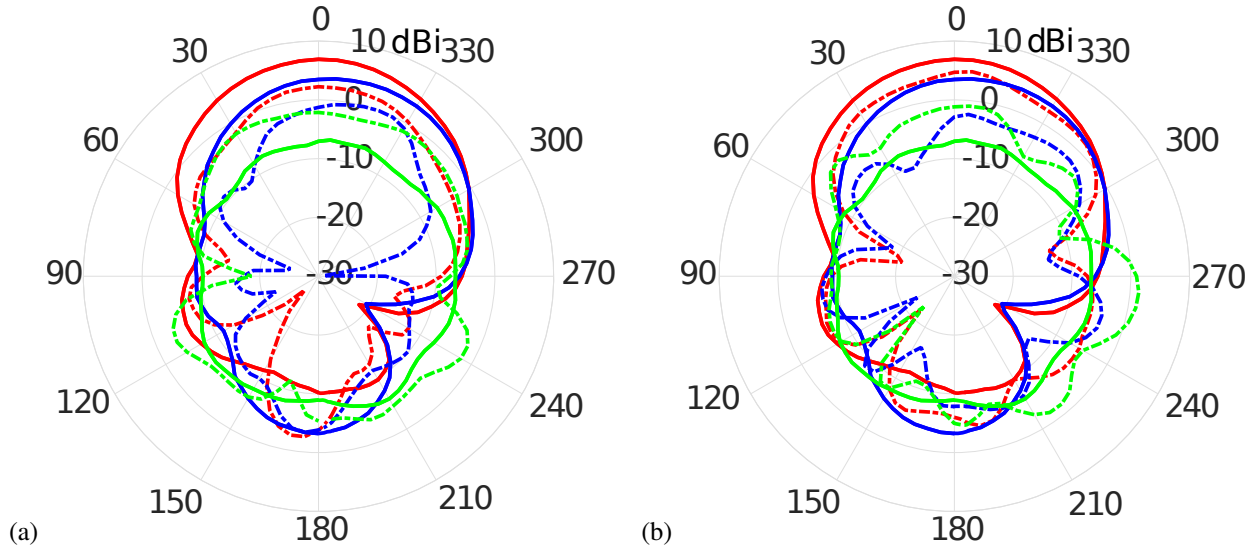

Fig. 4. Horizontal gain pattern (dB) of the E-shaped patch, the microstrip patch antenna, and the omnidirectional antenna in free space and attached to brick and cement board. Solid lines represent free space and dashed lines represent (a) brick and (b) cement board. The red lines represent E-shaped patch antenna, green lines represent omnidirectional antenna, and blue lines represent microstrip patch antenna.

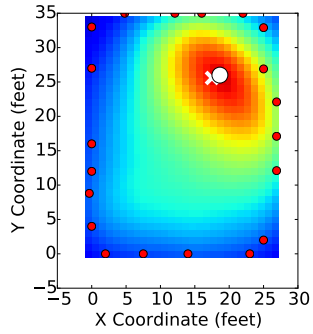

Fig. 5. An image generated by RTI during one of the experiments. The red circles are the nodes, the white X is true location, and the white circle is the estimated location.

The first method, which we call moving average-based RTI (MARTI), computes the absolute relative fractional change between a long and short term average RSS. In MARTI, we compute the link statistic for link l by first adding r_l into both a short and long term buffer where the length of the short and long term buffer can be tuned. We denote the average of the short term buffer as α_l and the average of the long term buffer as β_l. When a new r_l is measured, we compute the link statistic $y_l = |(\beta_l - \alpha_l)/\beta_l|$ [11].

The second method uses variance-based RTI (VRTI) [1] to compute the sample variance of a short buffer of RSS values. The length of the buffer can be tuned for optimal performance. When a new RSS measurement comes in for r_l, we add it to the buffer and let y_l equal the sample variance of the buffer.

V. Experimentation

To evaluate the performance of the proposed E-shaped patch antenna design, we perform a series of experiments at two different houses. In this section, we describe the hardware, the

pertinent information about the houses, and the test procedures we use to collect data used in post-processing.

A. Equipment

The wireless nodes deployed in the experiments use a Texas Instruments CC2530 radio module with an SMA interface to connect the antennas. We program twenty nodes to use a token passing protocol in a TDMA fashion to operate on four different channels in the 2.4 GHz ISM band. We package the nodes and antennas into sealed containers as shown in Fig. 6 and attach the container to the exterior walls so that the antennas' main lobe are directed into the house. We use our fabricated E-shaped patch antennas, microstrip patch antennas, and omnidirectional antennas. The nodes begin the communication protocol and an extra node is used to overhear the transmissions and save to file the measured RSS from each node. We note that a real-time implementation of RTI is possible, but post-processing is used in this paper for data analysis.

Fig. 6. The assembled node, antenna, and battery packet in an enclosure. These containers are then attached to the exterior walls with the antennas' main lobe directed inside the house.

B. Experiment Locations

We compare the performance of the antenna types at two different locations. The first house is a 875 square foot home whose exterior walls are made of brick. The home was fully furnished with beds, dressers, a kitchen table, a couch and two armchairs. The second house is a 1277 square foot home whose exterior walls are made of fiber cement siding which is a mixture of cement, sand and fibers. This house is also fully furnished. The two types of exterior walls gives us a way to demonstrate the E-shaped patch antenna's ability to keep its impedance tuned in the presence of different building materials. We choose these materials because of the houses' availability, however, we know from our testing that brick and cement board induce large losses in antenna gain and thus these are particularly challenging scenarios. The exterior walls of these two houses and the locations of the nodes are shown in Fig. 7.

C. Experiment Procedures

At each house, one experiment consists of a person walking inside at predefined locations at predefined times so that we know the ground truth location. When a new set of RSS measurements from each link is recorded, we compute the current link statistic vector $\mathbf{y}$ using both MARTI and VRTI,

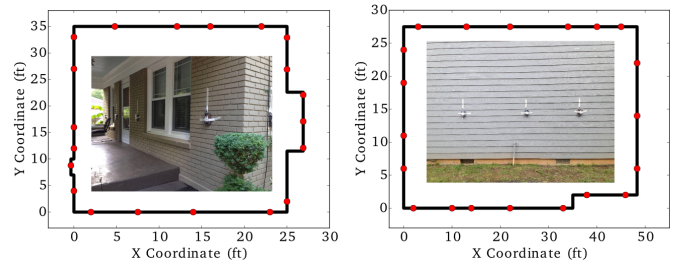

Fig. 7. Exterior walls and node coordinates with photo inset of (left) brick house and (right) cement board house.

and estimate the current location from $\hat{\mathbf{x}}$. We denote the current estimated location coordinates at sample time n as $\hat{\mathbf{w}}(n)$ and the true location coordinates as $\mathbf{w}(n)$. The RMSE is computed as

$$RMSE = \left[\frac{1}{E_{len}} \sum_{n=1}^{E_{len}} \|\hat{\mathbf{w}}(n) - \mathbf{w}(n)\|^2 \right]^{1/2} \tag{2}$$

where E_{len} is the number of link statistic vectors $\mathbf{y}$ computed during the experiment. At each house, three individuals perform two experiments each while the E-shaped patch antenna is installed. In the same fashion, we perform two more sets of six experiments, one for the microstrip patch antenna and another for the omnidirectional antenna. The time duration of each experiment is 3.5 minutes and so in total, we collect over 2 hours of RSS measurements which we make publicly available at [22].

VI. Results

In this section, we report the localization performance of each antenna type from our brick and cement board experiment sites. In addition, we show the localization performance of each antenna type as a function of the number of nodes deployed and the number of channels measured.

A. Overall Localization Performance

To compare the localization performance of each antenna, we take the median of the RMSE achieved over all six experiments that were performed using one antenna type. For reference, the minimum achievable median RMSE is 0.3 feet in the brick house and 0.35 feet in the cement board house using a 1 foot squared pixel. We show the median RMSE for the RTI methods in Fig. 8. We observe that the E-shaped patch antenna achieves a lower median RMSE than the other antennas using MARTI and VRTI in both the brick house and the cement board house. We show in Table I the percent decrease in median RMSE when comparing the E-shaped patch antenna to the omnidirectional and microstrip patch antenna. The E-shaped patch antenna reduces the median RMSE by more than 20% using either RTI method in the brick house with the microstrip patch antenna. The localization gains are more pronounced in the cement board house. The median RMSE, when using MARTI and the E-shaped patch, reduces by 37% compared to the omnidirectional antenna and 43% compared to the microstrip patch antenna.

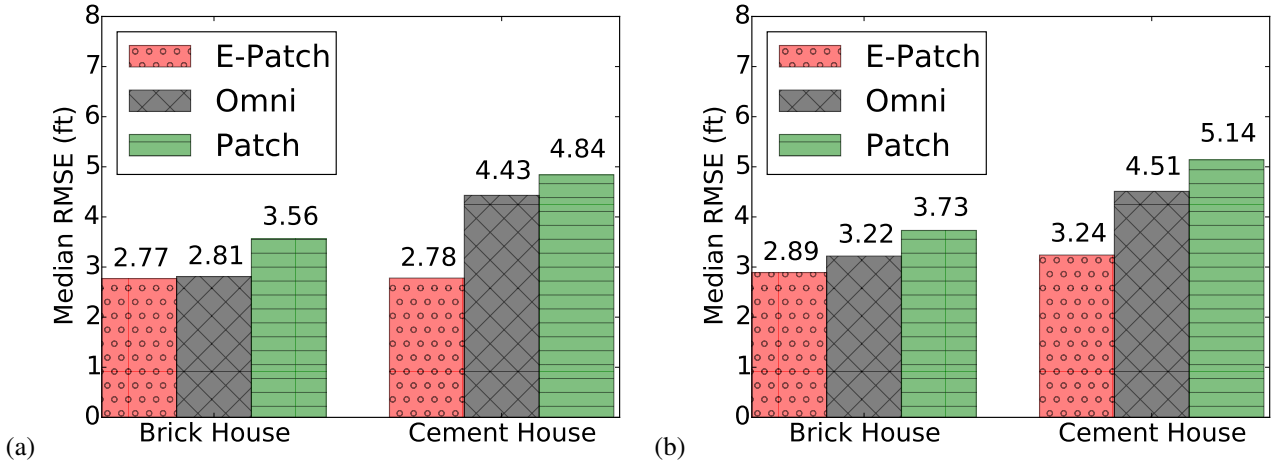

Fig. 8. Median RMSE achieved for a given antenna and material for (a) MARTI and (b) VRTI.

TABLE I
PERCENT DECREASE IN MEDIAN RMSE ACHIEVED BY USING E-SHAPED PATCH ANTENNA INSTEAD OF THE ANTENNA LISTED

	House	
RTI method and antenna type	Brick	Cement
MARTI with microstrip patch antenna	22	43
VRTI with microstrip patch antenna	23	37
MARTI with omnidirectional antenna	1	37
VRTI with omnidirectional antenna	10	28

We note that when we use MARTI in the brick house, the omnidirectional antenna performs almost as well as the E-shaped patch antenna. But this is not too surprising of a result since the size of the material and the dielectric properties can often work against one another to inadvertently make a resonance at the desired frequency of operation. We would expect a narrowband antenna to occasionally achieve a low median RMSE over a range of construction types and materials. But the E-shaped patch antenna is uniquely designed to capture a wide range of geometries and dielectric properties.

We also observe from Fig. 8 that the median RMSE achieved by the E-shaped patch antenna in the brick and cement house using either RTI method has a maximum difference of only 0.5 feet. In contrast, the difference for the omnidirectional antenna is 1.7 feet and 1.6 feet for the microstrip patch antenna. We see the E-shaped patch antenna makes through-wall RTI localization more robust across house size and building material compared to the omnidirectional and microstrip patch antenna.

The results shown in Fig. 8 are well explained by the measured reflection coefficient and radiation patterns shown in Figs. 3 and 4. We observe that the microstrip patch antenna's center frequency shifts away from 2.4 GHz after becoming detuned when it is placed against either brick or cement board. As a result, its median RMSE suffers the worst of all the antennas. One other interesting result is the lower median RMSE in the brick house compared to the cement house for all antenna types. Two factors that support our experimental results is that the reflection coefficients at 2.4 GHz for the antennas are lower in the brick house than the cement board house and that the brick house has a smaller footprint than cement board house. These results suggest that the size of the area being monitored and the building material both play a role in localization accuracy.

B. Localization Performance vs. Nodes Deployed

Although we deploy twenty nodes in our experiments, we wish to show how the median RMSE is affected when we deploy fewer nodes. To do this, we iterate through all combinations of $\binom{20}{a}$ nodes for $a \in \{16, 17, 18, 19, 20\}$ and compute the median RMSE over all iterations for a. We show the results in Fig. 9. From Fig. 9, we observe that the E-shaped patch antenna outperforms the other antenna types for any number of nodes deployed, for both RTI methods, and for both building materials. We also observe that, for all antenna types and building material, VRTI outperforms MARTI as the number of nodes decreases. The figure also shows that the percent increase of the median RMSE for using MARTI over VRTI at the brick house and using sixteen nodes is 31% for the mcirostrip patch antenna, 25% for the omnidirectional antenna, and 10% for the E-shaped patch antenna. If we instead use the cement house, the percent increase changes to 10% for the mcirostrip patch antenna, 13% for the omnidirectional antenna, and 13% for the E-shaped patch antenna. Our experimental results suggests that the percent increase in median RMSE with the E-shaped patch antenna is much less dependent on building material and RTI method than it is for the microstrip patch and omnidirectional antenna.

Another interesting result is that at the cement board house, the E-shaped patch antenna achieves the same median RMSE using sixteen nodes with VRTI and seventeen nodes with MARTI as the patch and omnidirectional antenna achieves with twenty nodes using either RTI method. Despite the cement board house's large footprint and the decreased number of nodes, the E-shaped patch antenna is still able to achieve similar or better localization performance than the other two antennas. Thus, we can use fewer nodes and consume less

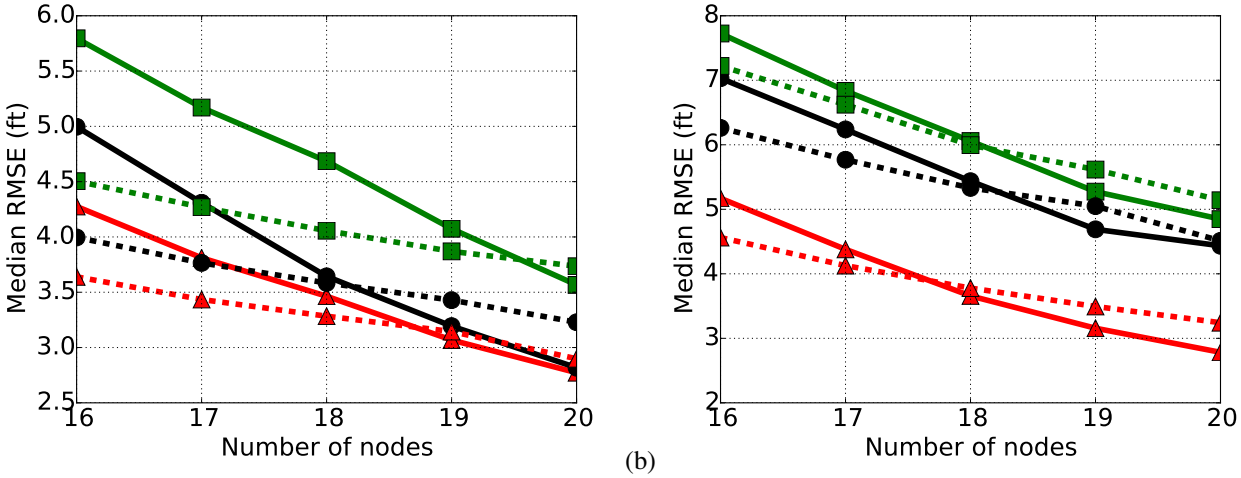

Fig. 9. Median RMSE achieved as a function of the number of nodes deployed for (a) brick house and (b) cement board house. Solid lines use MARTI while dashed lines use VRTI. The ▲ shows E-shaped patch antenna data points, ● shows omnidirectional antenna data points, and ■ shows microstrip patch antenna data points.

power by using the E-shaped patch antenna and still localize as well or better than when we use an omnidirectional or microstrip patch antenna.

C. Localization Performance vs. Channels Used

In our experiments, we program our nodes to measure on four channels in the 2.4 GHz band. But we are interested in how the median RMSE is influenced by the number of channels used. To do this, we iterate through all combinations of $\binom{4}{C}$ channels for $C \in \{1, 2, 3, 4\}$ and compute the median RMSE over all iterations for C. We show the results in Fig. 10. We observe that in all cases, the E-shaped patch antenna achieves a lower median RMSE than the omnidirectional and microstrip patch antenna. And in general, MARTI is a more robust localization method than VRTI when we measure RSS on fewer channels.

In the cement board house, we find that the we can measure on just one channel with the E-shaped patch and outperform the omnidirectional and microstrip patch antenna by 0.75 feet to 1.75 feet depending on the RTI method. In an application that is power-limited, the E-shaped patch antenna can achieve a lower RMSE but save power and bandwidth by only measuring on one channel. These power savings can also be seen if we consider both RTI methods and house types and only use the E-shaped patch antenna. We observe that in this case, using two channels instead of four only increases the median RMSE by up to 0.2 feet but reduces the power and bandwidth consumption by half.

VII. Future Work

There are some interesting ideas that are worth investigating in additional research. The first idea is that when nodes are placed against a wall in security or hostage scenarios, they may not be oriented in the correct way. The E-shaped patch antenna we use in this paper is linearly polarized. We were able to control the orientation of the antennas during the experiments so that polarization was not a concern. But in other cases, the antennas could be inadvertently oriented in a way that does not match the linearly polarization of the antenna, thus incurring losses. A possible solution is to create a circular polarized E-shaped patch antenna where the antennas could be oriented in any way on the exterior wall.

Another point of further investigation is how localization accuracy with RTI is a function of the link budget. We observed in Figs. 3 and 4 that the E-shaped patch antenna suffered the least loss in power when placed against a dielectric material and performed the best in terms of localization accuracy. To show that localization accuracy is a function of antenna design and not just received signal power, future work can simply reduce the transmit power of the nodes and perform a similar localization comparison of different antenna types.

VIII. Conclusion

In this paper, we presented improvements to through-wall RTI systems using a new E-shaped patch antenna. We designed the E-shaped patch to avoid impedance mismatches when placed in contact with an exterior wall. Avoiding impedance mismatches, along with its directionality, allow the E-shaped patch to radiate its power along the link line and improve localization. When compared to traditional omnidirectional and microstrip patch antennas, the E-shaped patch is more appropriate for use in security and first response scenarios where the antenna needs to be secured to an exterior wall.

We demonstrated that the E-shaped patch antenna reduced the median RMSE by up to 43% compared to a microstrip patch antenna and an omnidirectional antenna at a house made of brick and another made of cement board. The E-shaped patch antenna outperformed the other antennas in two studied RTI methods. We showed that the E-shaped patch antenna achieves a lower localization RMSE even when using fewer nodes and measuring RSS on fewer channels. These performance gains demonstrated that the E-shaped patch antenna can not only reduce localization errors, but it can do so on a tighter power and bandwidth budget. In applications where

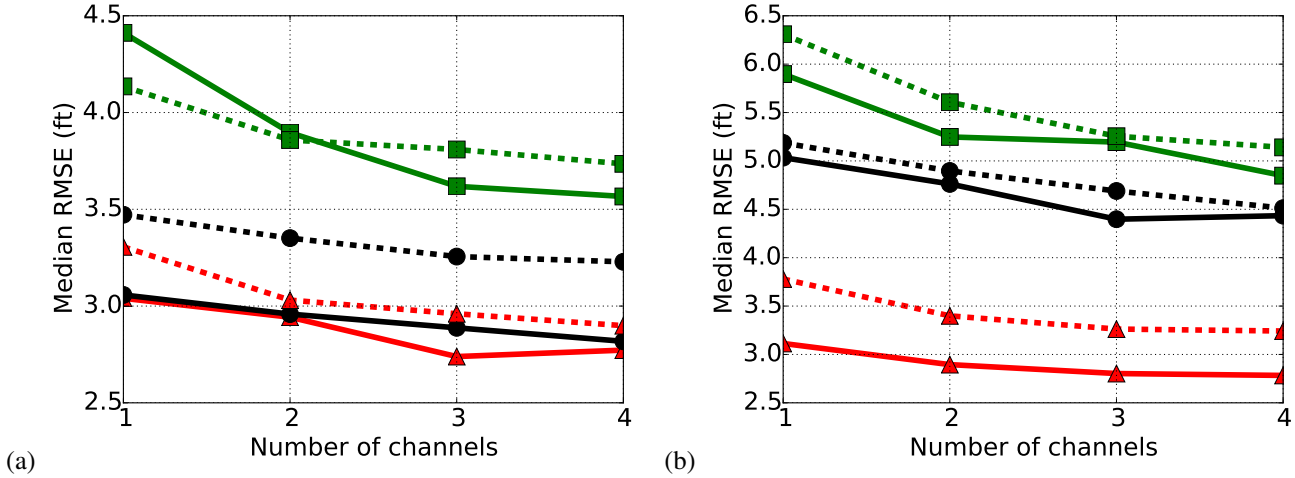

Fig. 10. Median RMSE achieved as a function of the number of channels measured for (a) brick house and (b) cement board house. Solid lines use MARTI while dashed lines use VRTI. The ▲ shows E-shaped patch antenna data points, ● shows omnidirectional antenna data points, and ■ shows microstrip patch antenna data points.

nodes are attached to the exterior wall of a building, the E-shaped patch can provide superior localization performance compared to other commonly used antennas.

Acknowledgment

This material is based upon work supported by the National Science Foundation under Grant Nos. #1407949 and #1408464. We would also like to thank Xandem Technology for lending the nodes we used during the experiments. And a special thanks to Charissa Che who provided invaluable editorial feedback.

References

[1] J. Wilson and N. Patwari, "See-through walls: Motion tracking using variance-based radio tomography networks," *IEEE Transactions on Mobile Computing*, vol. 10, no. 5, pp. 612–621, May 2011.

[2] M. McCracken, M. Bocca, and N. Patwari, "Joint ultra-wideband and signal strength-based through-building tracking for tactical operations," in *2013 IEEE International Conference on Sensing, Communications and Networking (SECON)*, June 2013, pp. 309–317.

[3] J. T. Gonzalez-Partida, P. Almorox-Gonzalez, M. Burgos-Garcia, B. P. Dorta-Naranjo, and J. I. Alonso, "Through-the-wall surveillance with millimeter-wave LFMCW radars," *IEEE Transactions on Geoscience and Remote Sensing*, vol. 47, no. 6, pp. 1796–1805, June 2009.

[4] J. Li, Z. Zeng, J. Sun, and F. Liu, "Through-wall detection of human being's movement by UWB radar," *IEEE Geoscience and Remote Sensing Letters*, vol. 9, no. 6, pp. 1079–1083, Nov 2012.

[5] D. Maas, J. Wilson, and N. Patwari, "Toward a rapidly deployable radio tomographic imaging system for tactical operations," in *IEEE SenseApp 2013*, Oct 2013, pp. 203–210.

[6] B. Wei, A. Varshney, N. Patwari, W. Hu, T. Voigt, and C. T. Chou, "dRTI: Directional radio tomographic imaging," in *Proceedings of the 14th International Conference on Information Processing in Sensor Networks*, ser. IPSN '15, 2015, pp. 166–177.

[7] Xandem Technology, "Xandem interview with swat commander - tactical through-wall tracking prototype," 2017. [Online]. Available: https://www.youtube.com/watch?v=QnQKfz-AEi4

[8] F. Yang, X.-X. Zhang, X. Ye, and Y. Rahmat-Samii, "Wide-band E-shaped patch antennas for wireless communications," *IEEE Transactions on Antennas and Propagation*, vol. 49, no. 7, pp. 1094–1100, Jul 2001.

[9] C. Qi, M. B. Akbar, and G. D. Durgin, "Analysis of E-patch antenna performance over various dielectric materials at 2.4 GHz," in *2016 IEEE International Symposium on Antennas and Propagation (APSURSI)*, June 2016, pp. 1807–1808.

[10] L. M. Ni, Y. Liu, Y. C. Lau, and A. P. Patil, "Landmarc: Indoor location sensing using active RFID," in *Proceedings of the First IEEE International Conference on Pervasive Computing and Communications, 2003. (PerCom 2003).*, March 2003, pp. 407–415.

[11] M. Youssef, M. Mah, and A. Agrawala, "Challenges: Device-free passive localization for wireless environments," in *Proceedings of the 13th Annual ACM International Conference on Mobile Computing and Networking*, ser. MobiCom '07, 2007, pp. 222–229.

[12] F. Viani, P. Rocca, M. Benedetti, G. Oliveri, and A. Massa, "Electromagnetic passive localization and tracking of moving targets in a WSN-infrastructured environment," *Inverse Problems*, vol. 26, no. 7, p. 074003, 2010.

[13] K. Woyach, D. Puccinelli, and M. Haenggi, "Sensorless sensing in wireless networks: Implementation and measurements," in *2006 4th International Symposium on Modeling and Optimization in Mobile, Ad Hoc and Wireless Networks*, April 2006, pp. 1–8.

[14] C. Xu, B. Firner, Y. Zhang, R. Howard, J. Li, and X. Lin, "Improving rf-based device-free passive localization in cluttered indoor environments through probabilistic classification methods," in *2012 ACM/IEEE 11th International Conference on Information Processing in Sensor Networks (IPSN)*, April 2012, pp. 209–220.

[15] B. Mager, P. Lundrigan, and N. Patwari, "Fingerprint-based device-free localization performance in changing environments," *IEEE Journal on Selected Areas in Communications*, vol. 33, no. 11, pp. 2429–2438, Nov 2015.

[16] J. Wilson and N. Patwari, "A fade-level skew-Laplace signal strength model for device-free localization with wireless networks," *IEEE Transactions on Mobile Computing*, vol. 11, no. 6, pp. 947–958, June 2012.

[17] X. Chen, A. Edelstein, Y. Li, M. Coates, M. Rabbat, and A. Men, "Sequential Monte Carlo for simultaneous passive device-free tracking and sensor localization using received signal strength measurements," in *Proceedings of the 10th ACM/IEEE International Conference on Information Processing in Sensor Networks*, April 2011, pp. 342–353.

[18] J. Wilson and N. Patwari, "Radio tomographic imaging with wireless networks," *IEEE Transactions on Mobile Computing*, vol. 9, no. 5, pp. 621–632, May 2010.

[19] O. Kaltiokallio, M. Bocca, and N. Patwari, "Enhancing the accuracy of radio tomographic imaging using channel diversity," in *2012 IEEE 9th International Conference on Mobile Ad-Hoc and Sensor Systems (MASS 2012)*, Oct 2012, pp. 254–262.

[20] L-Com Global Connectivity, "2.4 GHz 8 dBi LH Circular Polarized Patch Antenna - 4ft SMA Male Connector," 2017. [Online]. Available: http://www.l-com.com/wireless-antenna-24-ghz-8-dbi-lh-circular-polarized-patch-antenna-4ft-sma-male-connector

[21] J. Wilson, N. Patwari, and O. G. Vasquez, "Regularization methods for radio tomographic imaging," in *2009 Virginia Tech Symposium on Wireless Personal Communications*, 2009.

[22] P. Hillyard, "Data Set For Through-wall Localization Using an E-shaped Patch Antenna," 2017. [Online]. Available: http://bit.ly/2mzj4Ib